Metabolic phenotyping of healthy and diseased human RPE cells

Saira Rizwan[1,2*], Beverly Toothman[1,2*], Bo Li[1,2,3*], Abbi J. Engel[4], Rayne R. Lim[4], Sheldon Niernberger[4], Jinyu Lu[1,2], Cloe Ratliff[1,2], Yinxiao Xiang[1,2], Mark Eminhizer[1,2], Jennifer R. Chao[4&], and Jianhai Du[1,2&]

[1]Department of Ophthalmology and Visual Sciences, West Virginia University, Morgantown, WV 26506

[2]Department of Biochemistry and Molecular Medicine, West Virginia University, Morgantown, WV 26506

[3]Department of Ophthalmology, Affiliated Hospital of Yangzhou University, Yangzhou University, Yangzhou, Jiangsu Province 225100, China.

[4]Department of Ophthalmology, University of Washington, Seattle, WA 98109, United States.

[*]Equal contributions

[&]Corresponding Authors: Jianhai Du, One Medical Center Dr, PO Box 9193, WVU Eye Institute, Morgantown, WV 26505; Phone: (304)-293-9346; Fax; (304)-598-6928; Email: jianhai.du@hsc.wvu.edu; or Jennifer R. Chao: 750 Republican Street, Box 358058, Seattle WA 98109; Phone: (206) 221-0594. Email: jrchao@uw.edu.

Word count: 3473

Commercial relationships disclosures: None.

Funding: The funders had no role in the study design, data collection and analysis, decision on publishing, or manuscript preparation. This work was supported by National Institutes of Health Grant EY034364 (J. R. C. and J. D), EY03459 (J. R. C. and J. D), EY031324 (JD), EY032462(JD), the Retina Research Foundation (JD), UW Ophthalmology Stem Cell Fund (JRC), RPB Unrestricted Grant (UW), and funds for Core facilities P20 GM103434 and P20 GM144230 (WV INBRE grant).

Abstract (249 words)

Purpose: Metabolic defects in the retinal pigment epithelium (RPE) underlie many retinal degenerative diseases. This study aims to identify the nutrient requirements of healthy and diseased human RPE cells.

Methods: We profiled nutrient utilization of various human RPE cells, including differentiated and dedifferentiated fetal RPE (fRPE), induced pluripotent stem cell derived-RPE (iPSC RPE), Sorsby fundus dystrophy (SFD) patient-derived iPSC RPE, CRISPR-corrected isogenic SFD (cSFD) iPSC RPE, and ARPE-19 cell lines using Biolog Phenotype MicroArray Assays.

Results: Differentiated fRPE cells and healthy iPSC RPE cells can utilize 51 and 48 nutrients respectively, including sugars, intermediates from glycolysis and tricarboxylic acid (TCA) cycle, fatty acids, ketone bodies, amino acids, and dipeptides. However, when fRPE cells lose their epithelial phenotype through dedifferentiation, nutrient utilization becomes restricted to 17 nutrients, primarily sugar and glutamine-related amino acids. SFD RPE cells can utilize 37 nutrients; however, compared to cSFD RPE and healthy iPSC RPE, they are unable to utilize lactate, some TCA cycle intermediates, and short-chain fatty acids. Nonetheless, they show increased utilization of branch-chain amino acids (BCAAs) and BCAA-containing dipeptides. Dedifferentiated ARPE-19 cells grown in traditional culture media cannot utilize lactate and ketone bodies. In contrast, nicotinamide supplementation promotes differentiation towards an epithelial phenotype, restoring the ability to use these nutrients.

Conclusions: Epithelial phenotype confers metabolic flexibility to healthy RPE for utilizing various nutrients. SFD RPE cells have reduced metabolic flexibility, relying on the oxidation of BCAAs. Our findings highlight the potentially important roles of nutrient availability and utilization in RPE differentiation and diseases.

Introduction

Retinal pigment epithelium (RPE) is crucial in supporting photoreceptor function and survival through various functions, including the visual cycle, nutrient transport, light absorption, phagocytosis of outer segments, and formation of the blood-retina barrier[1]. To sustain these critical functions, the RPE relies on a robust mitochondrial metabolism by oxidizing fuels from the photoreceptors and choroidal supply[2]. Defects in RPE mitochondrial metabolism can cause epithelial-mesenchymal transition (EMT) and dedifferentiation, with loss of characteristic epithelial traits such as tight junctions, pigmentation and polarity, subsequently leading to photoreceptor death in retinal degenerative diseases, including Sorsby Fundus Dystrophy (SFD) and age-related macular degeneration (AMD)[2-4].

Cultured human RPE cells can be valuable models to investigate RPE function and retinal disease, as they exhibit typical RPE morphology, function and signature gene expression, which closely resemble native RPE cells[5-8]. Human fetal RPE (fRPE), patient-derived induced pluripotent stem cells (iPSC) RPE, and immortalized ARPE-19 cells are commonly used RPE cultures. Human fRPE cells have been rigorously characterized in their physiology, gene expression and metabolism, considered the gold standard in RPE culture[5, 9, 10]. iPSC RPE have been well-characterized and have the advantage of modeling inherited retinal diseases from patients. SFD, a rare early onset macular degeneration, results from mutations in the tissue inhibitor of metalloproteinase-3 (TIMP3) gene[11]. In our previous study, we showed that iPSC RPE derived from SFD patients carrying the S204C mutation in *TIMP3* have irregular extracellular matrices (ECM) and basal laminar deposits, while correction of the S204C variant in SFD iPSC RPE (cSFD) attenuates these findings[12]. ARPE-19 cells offer advantages over fRPE and iPSC RPE in terms of easier availability and low cost. ARPE-19 cells show fibroblast-like morphology under traditional culture media. However, supplementation with nicotinamide (NAM), a precursor for NAD, can rapidly induce differentiation of ARPE-19 cells into cells with many epithelial characteristics through revitalization of mitochondrial metabolism[13, 14].

In this study, we determined the metabolic phenotype of nutrient utilization in healthy and diseased human RPE. We conducted extensive metabolic screening of carbon and nitrogen sources across multiple human RPE cultures, including mature and dedifferentiated fRPE, healthy and SFD RPE, and ARPE-19 RPE cells under different culture media conditions. We found that healthy and mature RPE cells demonstrate robust metabolic flexibility, allowing them to utilize diverse nutrient sources. In contrast, dedifferentiated and SFD RPE cells have reduced metabolic flexibility, relying on specific nutrient sources. These cell-specific differences in nutrient utilization should provide insights into the underlying mechanisms of RPE differentiation and disease.

103

104 **Methods**

105 *Reagent and key resources*

106 All the reagents and key resources were detailed in Supplemental **Table S1** or methods.

107

108 *Human RPE cell culture*

109 Human fRPE was isolated from human fetal eye cups with no identifiers, obtained from two distinct
110 donors to the Birth Defects Research Laboratory at the University of Washington (UW) and cultured as
111 previously described[9, 15]. RPE cells at passages 4-6 were used for experiments, and they were seeded at a
112 density of either 5 x 10^4 cells/well (regular density) or 5 x 10^3 cells/well (low density) in 96-well plates in
113 MEM RPE media (See details in **Table S1**). iPSC RPE, one SFD patient-derived iPSC RPE cells and
114 CRISPR-corrected isogenic cSFD RPE cells were generated in a stepwise procedure as reported (see
115 details in Supplemental Methods)[12]. Human ARPE-19 cells obtained from the American Type Culture
116 Collection (ATCC) were used at passages 5-8 for the experiments. The cells were seeded at 2 x 10^4
117 cells/well in 96-well plates and cultured in three different media to mimic dedifferentiated and
118 differentiated states: 1) DMEM/F-12 media with 5% FBS, 2) MEM RPE media, and 3) MEM-NAM
119 (MEM RPE media supplemented with 10 mM NAM as reported[13, 14]. All RPE cells were cultured for 4
120 weeks metabolic screening.

121

122 *Metabolic screening with Biolog Phenotyping MicroArrays*

123 Biolog Phenotyping MicroArrays (Biolog Inc.) are 96-well plate assays that measure cellular metabolic
124 activity in utilizing various carbon and nitrogen substrates. Each well contains a specific nutrient at 100
125 μM concentration, except for the negative control. Cells are added to the 96-well in Biolog's proprietary
126 nutrient-limiting media, followed by the addition of a proprietary redox dye. This dye is reduced by
127 cellular NADH generated by substrate utilization, causing a color change measured by a plate reader.
128 High absorbance indicates greater metabolic activity in utilizing specific substrate through NADH
129 production. We used two Biolog Phenotype MicroArrays (PM-M1 for carbon sources and PM-M2 for
130 nitrogen sources) to assess nutrient utilization in RPE cells (see details in **Table S1-3**). After pre-
131 incubation with 60 uL of nutrient-limiting media (IFM 1, glutamine 200 μM, 1% dialyzed FBS, and 1%
132 penicillin and streptomycin) for one hour, RPE cell-containing plates were washed with PBS and
133 incubated with transferred pre-incubation media from PM-M1 or PM-M2 microarrays for 40 hours at
134 37ºC in a 5% CO_2 incubator. The redox dye mix MA (10 μL) was then added, and the plates were sealed
135 and read at an absorbance of 595 nm every 15 minutes for 4 hours.

136

137 *^{13}C glutamine tracing in fRPE cells*

138 Human fRPE cells seeded at regular and low densities were cultured for 4 weeks and changed into
139 DMEM with 5 mM glucose and 1 mM ^{13}C glutamine. After incubation for 48 hours, the RPE cells and
140 media were collected for metabolite extraction and analysis of ^{13}C glutamine-derived metabolites with gas
141 chromatography mass spectrometry (GC MS) as previously reported[9, 10].

142

143 *Statistics*

144 All data are expressed as the mean ± standard deviation. Fold change of absorbance over negative control
145 without nutrient source >1.5, or $p<0.05$ by Student's unpaired two-tailed t-tests using GraphPad Prism
146 9.0, was considered significant. Heat maps were generated in Microsoft Excel.

147

148 **Results**

149 *Mature human fRPE cells demonstrate remarkable metabolic flexibility in nutrient utilization.*

150 To study nutrient utilization in mature fRPE cells, fRPE were cultured for 4 weeks to maturity. RPE
151 demonstrated characteristic cobblestone morphology and pigmentation (Supplemental **Fig S1A-C**). The
152 mature RPE cultures were switched to nutrient-limiting media with or without a specific nutrient from the
153 PM-M1 plate to screen the utilization of 91 carbon sources (**Fig 1A, Table S2**). Remarkably, mature RPE
154 could utilize 23 carbon sources including sugars, glycolysis intermediates (such as sugar phosphates,
155 lactate, and pyruvate), TCA cycle intermediates, nucleosides, fatty acids and ketone bodies (**Fig 1B-C**). In
156 addition to glucose, mature RPE had the capacity to utilize other sugars such as fructose, mannose, and
157 galactose (**Fig 1B-C**). Nucleosides, containing ribose moiety, can serve as alternative energy sources.
158 Mature RPE could robustly utilize inosine, adenosine and uridine.

159

160 Similar to PM-M1 carbon source screening, we evaluated the utilization of 92 nitrogen sources, including
161 27 amino acids and 60 dipeptides in mature RPE using the PM-M2 plate as illustrated in **Fig 1D**. Mature
162 RPE could metabolize 7 amino acids and 17 dipeptides (**Fig 1E**). Except for methionine and tryptophan,
163 the remaining 5 amino acids (proline, ornithine, glutamine, glutamate, and aspartate) follow a similar
164 metabolic pathway in the generation of α-ketoglutarate (αKG) or oxaloacetate, which serve as fuels for
165 the TCA cycle (**Fig 1E, 1F**). Notably, glutamine, glutamate, aspartate, and proline are also present in the
166 17 dipeptides. These findings suggest that mature fRPE cells have remarkable metabolic flexibility,
167 enabling them to effectively utilize diverse nutrient sources to fuel their mitochondrial metabolism (**Fig**
168 **1C, 1E**).

169

170 *Dedifferentiated human fRPE cells lose metabolic flexibility, primarily relying on sugars and glutamine*
171 *as their main nutrient sources*.
172 Seeding fRPE at low density induces their dedifferentiation into a fibroblast-like phenotype[5]. To
173 understand nutrient utilization in dedifferentiated RPE cells, we seeded fRPE at 10% of regular density
174 and cultured them for 4 weeks. As expected, these cells transitioned from their characteristic cobblestone
175 structure to a fibroblast-like morphology, with upregulated expression of EMT markers including α-
176 smooth muscle actin (αSMA) and vimentin (**Fig 2A**, Supplemental **Fig S1D-F, Fig S2**). Total protein
177 content was similar in between mature and dedifferentiated RPE, indicating similar confluence between
178 culture conditions (**Fig S3**). Compared to mature fRPE, dedifferentiated fRPE utilized fewer nutrients,
179 with only 8 carbon and 6 nitrogen sources. Intriguingly, almost all carbon sources were sugar and sugar
180 phosphates, while all nitrogen sources contained glutamine (**Fig 2A-C**). These results suggest that
181 dedifferentiated RPE cells lose the ability to utilize multiple nutrient sources such as lactate, fatty acids,
182 ketone bodies and proline. Instead, they become largely restricted to consuming sugars and glutamine
183 (**Fig S4**). RPE seeded at low density for 1 week displayed a fibroblast-like morphology resembling that of
184 4-week cultured low-density fRPE cells but expressed less αSMA (**Fig S5A-B**, **Fig S1D-F, Fig S2**).
185 Nutrient utilization in 1-week cells was largely consistent with those of 4-week fRPE, except for the
186 capability to utilize galactose and adenosine at 1 week (**Fig S5B**), suggesting that time in culture has
187 minimal impact on the metabolic phenotype of nutrient utilization in RPE cells seeded at low density.
188 Consequently, we did not perform PM-M2 screening on 1-week fRPE.
189
190 To investigate how dedifferentiated RPE cells utilize glutamine, we incubated mature and dedifferentiated
191 RPE with ^{13}C glutamine for 48 hours and analyzed ^{13}C glutamine-derived intracellular and extracellular
192 metabolites (Fig 2D-E, Fig S6). Dedifferentiated RPE consumed more ^{13}C glutamine in the media, which
193 was utilized to produce mitochondrial intermediates and amino acids, especially succinate and proline
194 (Fig 2D-E, Fig S6). These results suggest that dedifferentiated RPE cells have an impaired electron
195 transport chain and reprogram their metabolism through reverse succinate dehydrogenase and proline
196 dehydrogenase towards succinate and proline production.
197
198 We next analyzed the expression of metabolic genes related to nutrient utilization in two RNA-Seq data
199 sets: 1) mature fRPE compared to dedifferentiated RPE induced by multiple passages[16] and 2) mature
200 primary adult RPE compared to dedifferentiated RPE induced by transforming growth factor-beta (TGFβ)
201 and tumor necrosis factor α (TNFα)[17]. Both dedifferentiated RPE models had significant downregulation
202 of genes involved in fatty acid oxidation, TCA cycle, transporters for lactate and ketone bodies,
203 nucleotide metabolism, and amino acid metabolism, especially proline catabolism and glutamine

204 synthetase (Fig 2F-G, **Table S4**). These data corroborate our findings that dedifferentiated RPE cannot
205 efficiently utilize fatty acids, lactate, ketone bodies, proline and other nucleosides for mitochondrial
206 metabolism. Importantly, genes involved in proline synthesis, glycolysis, collagen and heparin sulfate
207 were substantially upregulated (**Fig 2F**, **Table S4**), suggesting dedifferentiated RPE cells utilize sugar and
208 glutamine to activate proline synthesis and the hexosamine biosynthetic pathway to produce collagen and
209 glycan for ECM remodeling **(Fig 2F)**.
210
211 *Human iPSC RPE cells have similar metabolic flexibility to fRPE cells but utilize more sugars and TCA*
212 *cycle intermediates.*
213 To study nutrient utilization in human iPSC RPE cells, we cultured iPSC RPE to maturity at 4 weeks (**Fig**
214 **S7**) and then replaced media with carbon or nitrogen sources from PM-M1 or PM-M2 for metabolic
215 phenotyping (**Fig 3A**). iPSC RPE could utilize 31 carbon sources and 17 nitrogen sources (**Fig 3B-D**).
216 Similar to fRPE, iPSC RPE demonstrated robust flexibility in utilizing various sugars, fatty acids, lactate,
217 ketone bodies, nucleosides, amino acids, and dipeptides (**Fig 3B-D**). However, unlike fRPE, iPSC RPE
218 showed a utilization preference for more sugars and TCA cycle intermediates and fewer amino acids and
219 dipeptides (**Fig 3E-F**). These results suggest both healthy fRPE and iPSC RPE possess metabolic
220 flexibility in adapting to different substrates, yet also have cell type-specific preferences for certain
221 substrates.
222
223 *SFD iPSC RPE cells utilize fewer intermediates from glycolytic and TCA cycle intermediates but more*
224 *branch-chain amino acids (BCAAs)*.
225 We reported SFD iPSC RPE cells harboring the *TIMP3* S204 mutation have increased extracellular
226 deposits and elevated intracellular 4-hydroxyproline[12]. These iPSC RPE and their isogenic controls
227 (cSFD) were grown to maturity at 4 weeks before undergoing metabolic phenotyping with PM-M1 and
228 PM-M2 (**Fig 4A**). Both SFD and cSFD had normal cobblestone structure and pigmentation (**Fig S8A-B**).
229 SFD RPE utilized 19 carbon sources and 19 nitrogen sources, while cSFD RPE utilized 28 carbon sources
230 and 7 nitrogen sources (**Fig 4B-E**). SFD RPE utilized different types of sugar, nucleosides, fatty acids,
231 ketone bodies, amino acids and dipeptides (**Fig 4B, 4D**). However, SFD RPE could not utilize lactate,
232 sugar phosphate, short-chain fatty acids (acetate and butyrate), succinate, αKG and gamma-aminobutyric
233 acid (GABA). Notably, the CRISPR-corrected RPE cells restored the utilization of these nutrients (**Fig**
234 **4C-E**). SFD RPE could use proline and dipeptides containing glutamine, alanine and arginine.
235 Intriguingly, many of the dipeptides utilized by SFD RPE cells contained BCAAs, leucine, isoleucine and
236 valine, along with the ability to catabolize free leucine (**Fig 4D**). These metabolic phenotypes are
237 different from fRPE and normal control iPSC RPE. While the cSFD RPE cells did not use the BCAAs,

238 they also utilized significantly fewer nitrogen sources (**Fig 4E, Fig S8C**). These results suggest that SFD
239 RPE cells have metabolic defects in recycling nutrients, such as lactate from the neural retina, and rely
240 more on BCAAs, which may contribute to the formation of sub-RPE deposits of lipids and ECM proteins
241 (**Fig 4F**).
242
243 *Culture media composition controls the differentiation and nutrient utilization in ARPE-19 cells*.
244 ARPE-19 cells, typically cultured in DMEM/F-12 media per manufacturer's instructions, undergo rapid
245 differentiation into a mature RPE-like phenotype grown MEM-α-based RPE culture media supplemented
246 with NAM, [13, 14]. To investigate the influence of media composition on nutrient utilization, we cultured
247 ARPE-19 cells under three media (DMEM/F12, MEM RPE media and MEM RPE media plus NAM) for
248 4 weeks and focused only on the screening of carbon sources using the PM-M1 plate (**Fig 5A**). DMEM/F-
249 12 cultured cells (fibroblast-like morphology, **Fig S9A**) utilized 16 carbon sources (**Fig 5B**) but, similar to
250 dedifferentiated fRPE, could not metabolize lactate, ketone bodies, or xylitol (**Fig 5B, Fig 6A**). MEM
251 RPE media partially differentiated ARPE-19 cells (cobblestone structure, **Fig S9B**) and increased their
252 carbon source utilization to 24 (covering 94% of those used by DMEM/F12 cells, Fig 5C). While they
253 gained the ability to utilize ketone bodies and some sugars, lactate and xylitol remained unutilized (**Fig**
254 **5C**). Supplementation with NAM in MEM RPE media induced mature RPE-like morphology (**Fig S9C**)
255 and allowed ARPE-19 cells to utilize lactate, ketone bodies, sugar phosphates, xylose, and tagatose (**Fig**
256 **5D-E**). This metabolic phenotype resembles that of mature fRPE and iPSC RPE, although ARPE-19 cells
257 reduced utilization of short-chain fatty acids and maltose (**Fig 6A**). These findings highlight the critical
258 role of nutrient availability and utilization in RPE differentiation.
259
260 **Discussion**
261 In this study, we identified distinctive metabolic phenotypes of nutrient utilization in healthy and diseased
262 human RPE cells (**Fig 6**). Mature fRPE and iPSC RPE are metabolically flexible, capable of adapting to
263 various nutrient sources. Conversely, dedifferentiated RPE cells and SFD patient-derived iPSC RPE cells
264 have reduced flexibility and are biased towards fewer, specific substrates. Our findings suggest the critical
265 roles of nutrient utilization in RPE differentiation and dedifferentiation.
266
267 The RPE must manage a substantial nutrient influx originating daily from phagocytosed lipid- and
268 protein-rich photoreceptor outer segments, "waste products" such as lactate produced by the neural retina,
269 and nutrient-laden blood through the choroidal circulation[1, 2]. In addition to the direct transport of
270 nutrients to the neural retina, RPE can recycle and generate nutrients via lysosomes and mitochondria to
271 support retinal metabolism, thereby establishing a metabolic ecosystem between the outer retina and

272 RPE[1, 2, 18]. The ability to utilize a variety of nutrients is crucial for maintaining this metabolic ecosystem,
273 and disruption of this balance due to mitochondrial and/or lysosomal dysfunction in RPE can lead to
274 retinal degeneration[3, 4, 19]. Healthy human RPE cells are known to be versatile in utilizing different
275 nutrients, including glucose, galactose, lactate, fatty acids, succinate, proline, glutamine and other amino
276 acids[9, 18, 20-23]. Our results confirm this versatility, demonstrating that both healthy fRPE and iPSC RPE
277 cells are capable of utilizing these nutrients.
278
279 Furthermore, we found that human RPE cells utilize a wide range of other nutrients including various
280 sugars, ketone bodies, nucleosides and dipeptides. Mannose and galactose, for example, are components
281 of glycoproteins found in abundance in outer segment proteins such as rhodopsin and peripherin 2[24-26].
282 The ability to utilize these sugars from the daily degradation of outer segments may allow RPE to
283 preserve more glucose to supply for photoreceptors. Additionally, like the liver, human RPE cells can
284 synthesize ketone bodies, which can be utilized by the neural retina[21, 27]. Interestingly, we found that
285 mature human RPE, but not dedifferentiated RPE cells, can readily utilize ketone bodies, suggesting that
286 the ability to utilize ketone bodies might be a characteristic of RPE metabolism. Consistent with this
287 metabolic capability, mature RPE expresses key genes involved in ketone body degradation[21], a feature
288 distinct from the liver, which cannot utilize ketone bodies. Our findings underscore the metabolic
289 flexibility of healthy mature RPE in nutrient utilization, which is an essential function for RPE to support
290 retinal metabolism and health.
291
292 RPE EMT and dedifferentiation have been implicated in the pathogenesis of proliferative
293 vitreoretinopathy and AMD[28]. We found dedifferentiated RPE cells were unable to utilize alternative
294 fuels like lactate, fatty acids, ketone bodies and proline, but, instead, prefer to utilize sugars and
295 glutamine. RNA-seq data from EMT models show reduced expression of genes involved in the TCA
296 cycle, lactate transport, ketone body utilization and proline catabolism and glutamine synthesis. In
297 contrast, gene expression associated with glycolysis, proline synthesis, collagen synthesis and
298 glycoproteins are upregulated (**Fig 2E, Table S4**). Consistently, dedifferentiated RPE cells have been
299 reported to switch from oxidative phosphorylation to glycolysis and lose the ability to utilize proline as a
300 fuel[5, 15]. Inhibition of mitochondrial metabolism in human RPE cells or mouse RPE is sufficient to cause
301 the activation of glycolysis, RPE dedifferentiation and retinal degeneration[4, 29]. Furthermore,
302 mitochondrial respiration is diminished in cultured primary RPE cells from AMD donors[30]. Inhibiting
303 mitochondrial respiration impedes proline consumption while increasing glucose consumption and lactate
304 production[31]. The inability of affected RPE to utilize exogenous lactate and other alternative nutrient
305 sources may be an important mechanism in AMD pathogenesis.

306

307 A key feature in dedifferentiated cells is their overproduction of ECM proteins, primarily collagens and
308 glycoproteins, through activation of cytokine signaling such as TGFβ and TNFα[32, 33]. In fibroblasts, TGFβ
309 stimulates the oxidation of glucose and glutamine to synthesize proline and other amino acids crucial for
310 ECM protein production[34]. Interestingly, proline synthesis acts as a vent for growth when cells are under
311 mitochondrial redox stress or hypoxia by recycling NADH into NAD^+, thus enhancing the oxidation of
312 glutamine and glucose[34, 35]. Proline synthesis may be particularly crucial in dedifferentiated RPE cells,
313 given their inhibited mitochondrial metabolism and heavy reliance on lactate production for NAD^+
314 regeneration. Similarly, to compensate for the deficiency in the electron transport chain or hypoxia,
315 fumarate can serve as an electron acceptor to produce succinate[36], which is accumulated in
316 dedifferentiated RPE. Strategies aimed at relieving mitochondrial redox stress and reverting proline
317 synthesis to proline catabolism or succinate production could hold promise for treating RPE
318 dedifferentiation.

319

320 *TIMP3*, a risk gene for AMD, is secreted by the RPE and plays a critical role in ECM remodeling by
321 inhibiting matrix metalloproteinases[37]. Specific mutations in *TIMP3* result in SFD, which is characterized
322 by a thickened layer of basal laminar drusen-like sub-RPE deposits containing lipids and ECM proteins[12,
323 38]. Unlike healthy or mutation-corrected RPE cells, SFD RPE cells utilize more free BCAAs or dipeptides
324 containing BCAAs (**Fig 4F, Fig 6**). Leucine and isoleucine are ketogenic amino acids, and their oxidation
325 promotes the synthesis and transport of fatty acids and cholesterol[39, 40]. BCAA oxidation is closely
326 associated with dysregulated glucose and lipid metabolism in diabetes and non-alcoholic fatty liver
327 diseases[39, 41, 42]. Interestingly, intermediates of the BCAA degradation pathway are significantly elevated
328 in the plasma of AMD patients[43], and *BCAT1*, a key gene in BCAA degradation, is upregulated in the
329 RPE/choroid from AMD donors[44]. Moreover, in addition to proline, ECM proteins are highly enriched in
330 BCAAs[45]. Our findings suggest that SFD RPE may upregulate the BCAA degradation pathway by
331 utilizing BCAAs from free amino acids or protein degradation, contributing to the formation of sub-RPE
332 deposits.

333

334 There are a few limitations in this study. We did not normalize nutrient utilization to specific cell
335 numbers, although total cellular protein content was similar between dedifferentiated and mature RPE by
336 4 weeks in culture. Nutrient utilization in additional dedifferentiation models need to be conducted in
337 future studies. Separately, high absorbance reflects greater reduction of NADH generated from a specific
338 nutrient. The Biolog assays cannot detect the reduction of FADH2 or other metabolic pathways such as
339 the synthesis of amino acids, nucleotides and fatty acids. In addition, the metabolic phenotyping assay

can only measure the capability and capacity of utilizing a specific nutrient but not preferences of nutrient utilization because only one nutrient is available at a time. Therefore, the utilization might be different *in vivo*, and additional functional studies with nutrient supplements or genetic manipulations of metabolic pathways are needed to interpret these findings. Finally, testing additional iPSC RPE lines from a larger cohort of normal and affected donors will help control for variability in genetic and environmental backgrounds.

In conclusion, metabolic phenotyping offers a sensitive and powerful platform for measuring nutrient utilization in healthy and diseased human RPE cells. The distinct patterns of nutrient utilization of various RPE cells provide valuable insights into the mechanisms of RPE dedifferentiation and disease.

Acknowledgments

This work was supported by National Institutes of Health Grant EY034364 (J. R. C. and J. D), EY03459 (J. R. C. and J. D), EY031324 (JD), EY032462(JD), the Retina Research Foundation (JD), and funds for Core facilities P20 GM103434 and P20 GM144230 (WV INBRE grant). Fetal RPE tissue samples were made available through Dr. Ian Glass and the Birth Defects Research Laboratory at the University of Washington (UWR24HD000836).

Conflicts of interest

The authors declare no conflicts of interest.

References

1. Lakkaraju A, Umapathy A, Tan LX, et al. The cell biology of the retinal pigment epithelium. *Prog Retin Eye Res* 2020;100846.
2. Hurley JB. Retina Metabolism and Metabolism in the Pigmented Epithelium: A Busy Intersection. *Annu Rev Vis Sci* 2021;7:665-692.
3. Ferrington DA, Fisher CR, Kowluru RA. Mitochondrial Defects Drive Degenerative Retinal Diseases. *Trends Mol Med* 2020;26:105-118.
4. Zhao C, Yasumura D, Li X, et al. mTOR-mediated dedifferentiation of the retinal pigment epithelium initiates photoreceptor degeneration in mice. *J Clin Invest* 2011;121:369-383.
5. Adijanto J, Philp NJ. Cultured primary human fetal retinal pigment epithelium (hfRPE) as a model for evaluating RPE metabolism. *Exp Eye Res* 2014;126:77-84.
6. Bharti K, den Hollander AI, Lakkaraju A, et al. Cell culture models to study retinal pigment epithelium-related pathogenesis in age-related macular degeneration. *Exp Eye Res* 2022;222:109170.
7. Nazari H, Zhang L, Zhu D, et al. Stem cell based therapies for age-related macular degeneration: The promises and the challenges. *Prog Retin Eye Res* 2015;48:1-39.

378 8. Blenkinsop TA, Saini JS, Maminishkis A, et al. Human Adult Retinal Pigment Epithelial Stem Cell-
379 Derived RPE Monolayers Exhibit Key Physiological Characteristics of Native Tissue. *Invest Ophthalmol Vis*
380 *Sci* 2015;56:7085-7099.
381 9. Chao JR, Knight K, Engel AL, et al. Human retinal pigment epithelial cells prefer proline as a
382 nutrient and transport metabolic intermediates to the retinal side. *J Biol Chem* 2017;292:12895-12905.
383 10. Du J, Zhu S, Lim RR, Chao JR. Proline metabolism and transport in retinal health and disease.
384 *Amino Acids* 2021;53:1789-1806.
385 11. Anand-Apte B, Chao JR, Singh R, Stohr H. Sorsby fundus dystrophy: Insights from the past and
386 looking to the future. *J Neurosci Res* 2019;97:88-97.
387 12. Engel AL, Wang Y, Khuu TH, et al. Extracellular matrix dysfunction in Sorsby patient-derived
388 retinal pigment epithelium. *Exp Eye Res* 2022;215:108899.
389 13. Hazim RA, Volland S, Yen A, Burgess BL, Williams DS. Rapid differentiation of the human RPE cell
390 line, ARPE-19, induced by nicotinamide. *Exp Eye Res* 2019;179:18-24.
391 14. Hazim RA, Paniagua AE, Tang L, et al. Vitamin B3, nicotinamide, enhances mitochondrial
392 metabolism to promote differentiation of the retinal pigment epithelium. *J Biol Chem* 2022;298:102286.
393 15. Yam M, Engel AL, Wang Y, et al. Proline mediates metabolic communication between retinal
394 pigment epithelial cells and the retina. *J Biol Chem* 2019;294:10278-10289.
395 16. Radeke MJ, Radeke CM, Shih YH, et al. Restoration of mesenchymal retinal pigmented epithelial
396 cells by TGFbeta pathway inhibitors: implications for age-related macular degeneration. *Genome Med*
397 2015;7:58.
398 17. Boles NC, Fernandes M, Swigut T, et al. Epigenomic and Transcriptomic Changes During Human
399 RPE EMT in a Stem Cell Model of Epiretinal Membrane Pathogenesis and Prevention by Nicotinamide.
400 *Stem Cell Reports* 2020;14:631-647.
401 18. Kanow MA, Giarmarco MM, Jankowski CS, et al. Biochemical adaptations of the retina and
402 retinal pigment epithelium support a metabolic ecosystem in the vertebrate eye. *Elife* 2017;6.
403 19. Boya P, Kaarniranta K, Handa JT, Sinha D. Lysosomes in retinal health and disease. *Trends*
404 *Neurosci* 2023;46:1067-1082.
405 20. Liu B, Calton MA, Abell NS, et al. Genetic analyses of human fetal retinal pigment epithelium
406 gene expression suggest ocular disease mechanisms. *Commun Biol* 2019;2:186.
407 21. Adijanto J, Du J, Moffat C, Seifert EL, Hurle JB, Philp NJ. The retinal pigment epithelium utilizes
408 fatty acids for ketogenesis. *J Biol Chem* 2014;289:20570-20582.
409 22. Bisbach CM, Hass DT, Robbings BM, et al. Succinate Can Shuttle Reducing Power from the
410 Hypoxic Retina to the O(2)-Rich Pigment Epithelium. *Cell Rep* 2020;31:107606.
411 23. Li B, Zhang T, Liu W, et al. Metabolic Features of Mouse and Human Retinas: Rods versus Cones,
412 Macula versus Periphery, Retina versus RPE. *iScience* 2020;23:101672.
413 24. Skiba NP, Lewis TR, Spencer WJ, Castillo CM, Shevchenko A, Arshavsky VY. Absolute
414 Quantification of Photoreceptor Outer Segment Proteins. *J Proteome Res* 2023;22:2703-2713.
415 25. Stuck MW, Conley SM, Naash MI. PRPH2/RDS and ROM-1: Historical context, current views and
416 future considerations. *Prog Retin Eye Res* 2016;52:47-63.
417 26. Daniele LL, Han JYS, Samuels IS, et al. Glucose uptake by GLUT1 in photoreceptors is essential for
418 outer segment renewal and rod photoreceptor survival. *FASEB J* 2022;36:e22428.
419 27. Reyes-Reveles J, Dhingra A, Alexander D, Bragin A, Philp NJ, Boesze-Battaglia K. Phagocytosis-
420 dependent ketogenesis in retinal pigment epithelium. *J Biol Chem* 2017;292:8038-8047.
421 28. Zhou M, Geathers JS, Grillo SL, et al. Role of Epithelial-Mesenchymal Transition in Retinal
422 Pigment Epithelium Dysfunction. *Front Cell Dev Biol* 2020;8:501.
423 29. Hu X, Calton MA, Tang S, Vollrath D. Depletion of Mitochondrial DNA in Differentiated Retinal
424 Pigment Epithelial Cells. *Sci Rep* 2019;9:15355.

425 30. Fisher CR, Ferrington DA. Perspective on AMD Pathobiology: A Bioenergetic Crisis in the RPE.
426 *Invest Ophthalmol Vis Sci* 2018;59:AMD41-AMD47.
427 31. Zhang R, Engel AL, Wang Y, et al. Inhibition of Mitochondrial Respiration Impairs Nutrient
428 Consumption and Metabolite Transport in Human Retinal Pigment Epithelium. *J Proteome Res*
429 2021;20:909-922.
430 32. Scott LE, Weinberg SH, Lemmon CA. Mechanochemical Signaling of the Extracellular Matrix in
431 Epithelial-Mesenchymal Transition. *Front Cell Dev Biol* 2019;7:135.
432 33. Shu DY, Butcher E, Saint-Geniez M. EMT and EndMT: Emerging Roles in Age-Related Macular
433 Degeneration. *Int J Mol Sci* 2020;21.
434 34. Schworer S, Berisa M, Violante S, et al. Proline biosynthesis is a vent for TGFbeta-induced
435 mitochondrial redox stress. *EMBO J* 2020;39:e103334.
436 35. Westbrook RL, Bridges E, Roberts J, et al. Proline synthesis through PYCR1 is required to support
437 cancer cell proliferation and survival in oxygen-limiting conditions. *Cell Rep* 2022;38:110320.
438 36. Spinelli JB, Rosen PC, Sprenger HG, et al. Fumarate is a terminal electron acceptor in the
439 mammalian electron transport chain. *Science* 2021;374:1227-1237.
440 37. Alexander JP, Bradley JM, Gabourel JD, Acott TS. Expression of matrix metalloproteinases and
441 inhibitor by human retinal pigment epithelium. *Invest Ophthalmol Vis Sci* 1990;31:2520-2528.
442 38. Weber BH, Vogt G, Pruett RC, Stohr H, Felbor U. Mutations in the tissue inhibitor of
443 metalloproteinases-3 (TIMP3) in patients with Sorsby's fundus dystrophy. *Nat Genet* 1994;8:352-356.
444 39. Neinast MD, Jang C, Hui S, et al. Quantitative Analysis of the Whole-Body Metabolic Fate of
445 Branched-Chain Amino Acids. *Cell Metab* 2019;29:417-429 e414.
446 40. Jang C, Oh SF, Wada S, et al. A branched-chain amino acid metabolite drives vascular fatty acid
447 transport and causes insulin resistance. *Nat Med* 2016;22:421-426.
448 41. White PJ, McGarrah RW, Grimsrud PA, et al. The BCKDH Kinase and Phosphatase Integrate BCAA
449 and Lipid Metabolism via Regulation of ATP-Citrate Lyase. *Cell Metab* 2018;27:1281-1293 e1287.
450 42. White PJ, Lapworth AL, An J, et al. Branched-chain amino acid restriction in Zucker-fatty rats
451 improves muscle insulin sensitivity by enhancing efficiency of fatty acid oxidation and acyl-glycine
452 export. *Mol Metab* 2016;5:538-551.
453 43. Haijes HA, Jans JJM, van der Ham M, van Hasselt PM, Verhoeven-Duif NM. Understanding acute
454 metabolic decompensation in propionic and methylmalonic acidemias: a deep metabolic phenotyping
455 approach. *Orphanet J Rare Dis* 2020;15:68.
456 44. Newman AM, Gallo NB, Hancox LS, et al. Systems-level analysis of age-related macular
457 degeneration reveals global biomarkers and phenotype-specific functional networks. *Genome Med*
458 2012;4:16.
459 45. Li P, Wu G. Roles of dietary glycine, proline, and hydroxyproline in collagen synthesis and animal
460 growth. *Amino Acids* 2018;50:29-38.
461

462 **Figure legends**

463 **Figure 1. Metabolic phenotyping of mature human fRPE cells.** (A) A schematic for metabolic
464 phenotyping with carbon sources. Human fRPE cells were grown for 4 weeks in a 96-well plate and then
465 switched into nutrient-limiting media containing different carbon sources in each well from PM-M1 plate.
466 The utilization of nutrients leads to NADH production, casuing a color change in a redox sensitive dye to
467 purple, which is quantified by a microplate reader at 595 nm. (B) The utilization of carbon sources by
468 mature human fRPE cells and (C) an illustration of the metabolic pathways. (D) A schematic for
469 metabolic phenotyping of nitrogen sources using PM-M2. (E) The utilization of nitrogen sources by

470 mature human fRPE cells and (F) an illustration of the metabolic pathways. N=3. Fold change over
471 negative control without nutrient source (Ctr)>1.5 or *P<0.05 over Ctr. Gluc, Glucose, Gal, galactose;
472 Mann, Mannose; F1P, fructose 1-phosphophate; R1P, ribose 1-phosphate, G6P, glucose 3-phosphate;
473 G3P, glycerol 3-phosphate; AcAc, Acetoacetic Acid; 3HB, β-Hydroxy Butyrate; MelA, Melibionic Acid.
474
475
476 **Figure 2**. **Metabolic phenotyping of dedifferentiated human fRPE.** (A) Human fRPE were seeded at
477 low density to induce dedifferentiation with a mesenchymal phenotype in a 96-well plate and then
478 switched into nutrient-limiting media containing different carbon (PM-M1) or nitrogen sources (PM-M2)
479 for metabolic phenotyping. (B) Nutrient utilization of carbon sources by dedifferentiated human fRPE.
480 N=4. Fold change>1.5 or P<0.05 over Ctr. (C) Nutrient utilization of nitrogen sources by dedifferentiated
481 human fRPE. N=3. Fold change>1.5 or P<0.05 over Ctr. (D-E) Dedifferentiated RPE consumes more
482 glutamine for their mitochondrial metabolism. ^{13}C-glutamine and its derived metabolites in media (D) and
483 RPE cells (E) were analyzed by GC MS and presented as fold change of ^{13}C labeled abundance over low
484 density RPE. N=4. *P<0.05 vs mature RPE. (F) Heat maps of altered metabolic genes in dedifferentiated
485 RPE cells induced by TNT (left panel) or multiple passage (right panel) (G) The dedifferentiated RPE
486 cells lose the ability to utilize multiple nutrient sources but switch to use glutamine, enhancing proline
487 and collagen synthesis. Magenta denotes an increase and blue denotes a decrease in gene expression or
488 metabolic pathways. *PFKFB4*, 6-phosphofructo-2-kinase/fructose-2,6-bisphosphatase 4, *LDHA*, Lactate
489 dehydrogenase A; *OGDH*, Oxoglutarate dehydrogenase; *PRODH*; Proline dehydrogenase; *PYCR1*,
490 Pyrroline-5-carboxylate reductase 1; P4H4, Prolyl 4-hydroxylase subunit alpha or beta; *GMPPA*, GDP-
491 mannose pyrophosphorylase A. *PMM2*, Phosphomannomutase 2.
492
493 **Figure 3. Metabolic phenotyping of healthy human iPSC RPE cells. (A)** Human iPSC RPE cells were
494 differentiated in RPE media for 4 weeks and switched into nutrient-limit media from PM1 or PM2 for
495 metabolic phenotyping. (B-D) Nutrient utilization of carbon sources and nitrogen sources by human iPSC
496 RPE cells. N=3. Fold change>1.5 or P<0.05 over Ctr. (E) A comparison of number of nutrients that were
497 utilized between fRPE and iPSC RPE cells. (F) An illustration of nutrient utilization in iPSC RPE cells.
498 GlcNAc, N-Acetyl-D-Glucosamine; Tcba, Tricarballylic Acid; AlaN, L-Alaninamide.
499
500 **Figure 4. Metabolic phenotyping of IPSC SFD and cSFD RPE cells.** (A) Human iPSC SFD RPE
501 carrying TIMP3 S204C mutation and mutation corrected cSFD RPE cells were differentiated in RPE
502 media for 4 weeks and then switched to nutrient-limit media with carbon or nitrogen sources from PM-
503 M1 or PM-M2 for metabolic phenotyping. (B-E) Nutrient utilization of (B-C) carbon sources and (D-E)

504 nitrogen sources in iPSC SFD RPE cells. N=3. Fold change>1.5 or P<0.05 over Ctr. (F) An illustration of
505 altered nutrient utilization in SFD iPSC RPE cells. L-Mal, L-Malic Acid; mmSuc, mono methyl
506 succinate; 3HB, β-Hydroxy Butyrate; BCAAs, Branch-Chained Amino Acids.
507
508
509 **Figure 5. Metabolic phenotyping of ARPE-19 cells cultured in different media.**
510 (A) ARPE-19 cells were cultured in three different media: DMEM/F-12, MEM RPE media, and MEM
511 RPE media with 10 mM NAM for 4 weeks. All the cells were then changed into nutrient-limit media with
512 carbon sources from PM-M1 for metabolic phenotyping. (B-D) Nutrient utilization of carbon sources of
513 ARPE-19 cells cultured in (B) DMEM/F12 (C) MEM RPE media, (D) MEM RPE media with NAM.
514 Fold change>1.5 or P<0.05 over Ctr. (E) A comparison of number of nutrients that were utilized in
515 ARPE-19 cells grown in different culture media. (F-G) An illustration of altered nutrient utilization in
516 APRE-19 cells cultured between DMEM/F12 and MEM RPE media with NAM. Meso-Tar, Meso Tartatic
517 acid; mmSuc, mono methyl succinate; AcAc, Acetoacetic Acid; 3HB, β-Hydroxy Butyrate.
518
519 **Figure 6. Comparison of metabolic phenotyping profiles of human fRPE cells, dedifferentiated**
520 **fRPE, iPSC RPE cells, SFD RPE, cSFD RPE and ARPE-19 cells grown under different culture**
521 **media.** Heat map visualization of nutrients that were differentially utilized by different RPE cells from
522 (A) PM-M1 nutrients and (B) PM-M2 nutrient microarray plates. De-fRPE, dedifferentied fRPW with
523 low density seedings; ARPE, ARPE-19 cells; MelA, Melibionic Acid; GlcNAc, N-Acetyl-D-
524 Glucosamine; Tcba, Tricarballylic acid; mmSuc, mono methyl succinate; AlaN, Alaninamide.
525
526
527
528
529
530
531
532
533
534
535
536

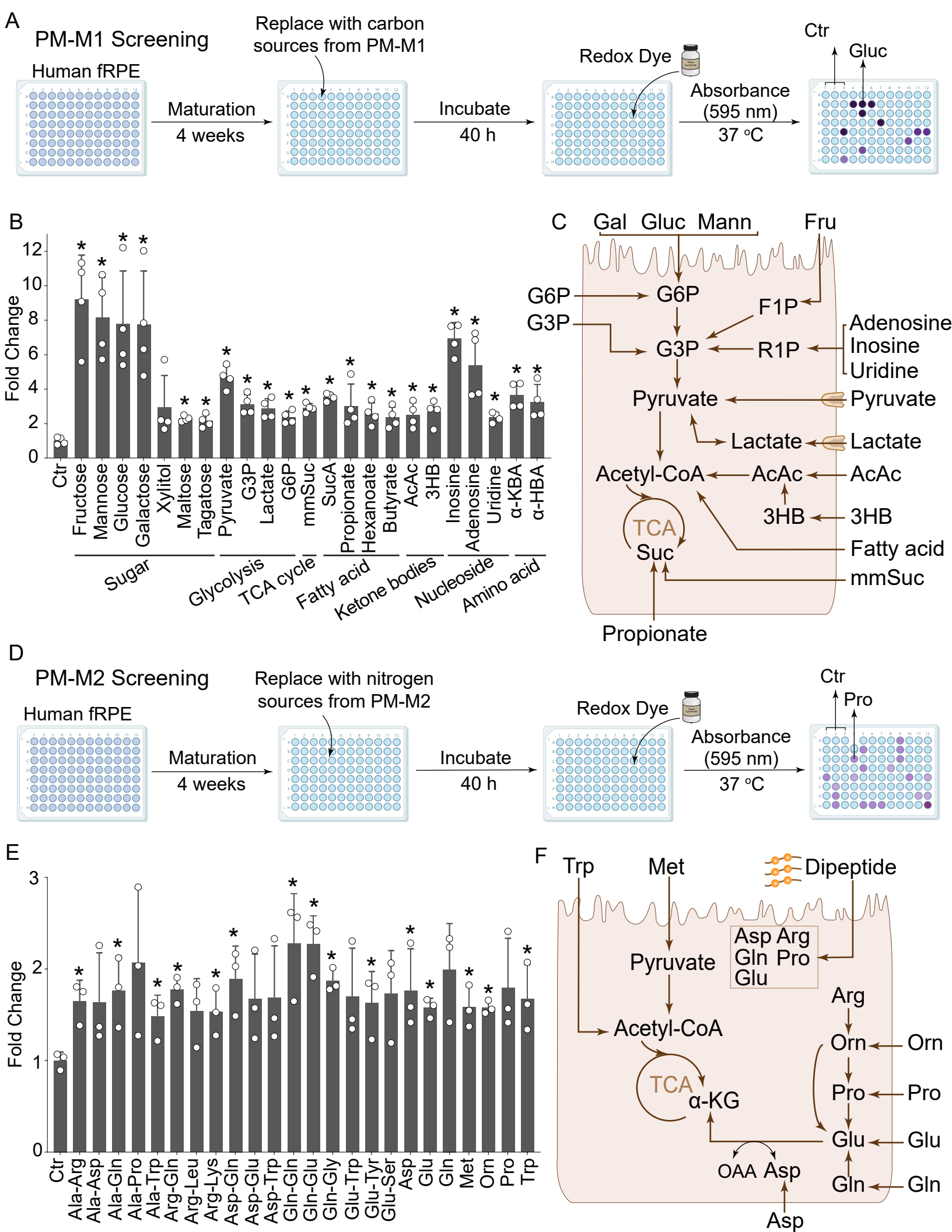
A
PM-M1 Screening
Human fRPE
Maturation
4 weeks
Replace with carbon sources from PM-M1
Incubate
40 h
Redox Dye
Absorbance (595 nm)
37 °C
Ctr
Gluc
B
Fold Change
Ctr
Fructose
Mannose
Glucose
Galactose
Xylitol
Maltose
Tagatose
Pyruvate
G3P
Lactate
G6P
mmSuc
SucA
Propionate
Hexanoate
Butyrate
AcAc
3HB
Inosine
Adenosine
Uridine
α-KBA
α-HBA
Sugar
Glycolysis
TCA cycle
Fatty acid
Ketone bodies
Nucleoside
Amino acid
C
Gal
Gluc
Mann
Fru
G6P
G3P
F1P
R1P
Adenosine
Inosine
Uridine
Pyruvate
Lactate
Acetyl-CoA
AcAc
3HB
TCA
Suc
Fatty acid
mmSuc
Propionate
D
PM-M2 Screening
Human fRPE
Maturation
4 weeks
Replace with nitrogen sources from PM-M2
Incubate
40 h
Redox Dye
Absorbance (595 nm)
37 °C
Ctr
Pro
E
Fold Change
Ctr
Ala-Arg
Ala-Asp
Ala-Gln
Ala-Pro
Ala-Trp
Arg-Gln
Arg-Leu
Arg-Lys
Asp-Gln
Asp-Glu
Asp-Trp
Gln-Gln
Gln-Glu
Gln-Gly
Glu-Trp
Glu-Tyr
Glu-Ser
Asp
Glu
Gln
Met
Orn
Pro
Trp
F
Trp
Met
Dipeptide
Asp Arg
Gln Pro
Glu
Pyruvate
Acetyl-CoA
TCA
α-KG
Arg
Orn
Pro
Glu
Gln
OAA
Asp

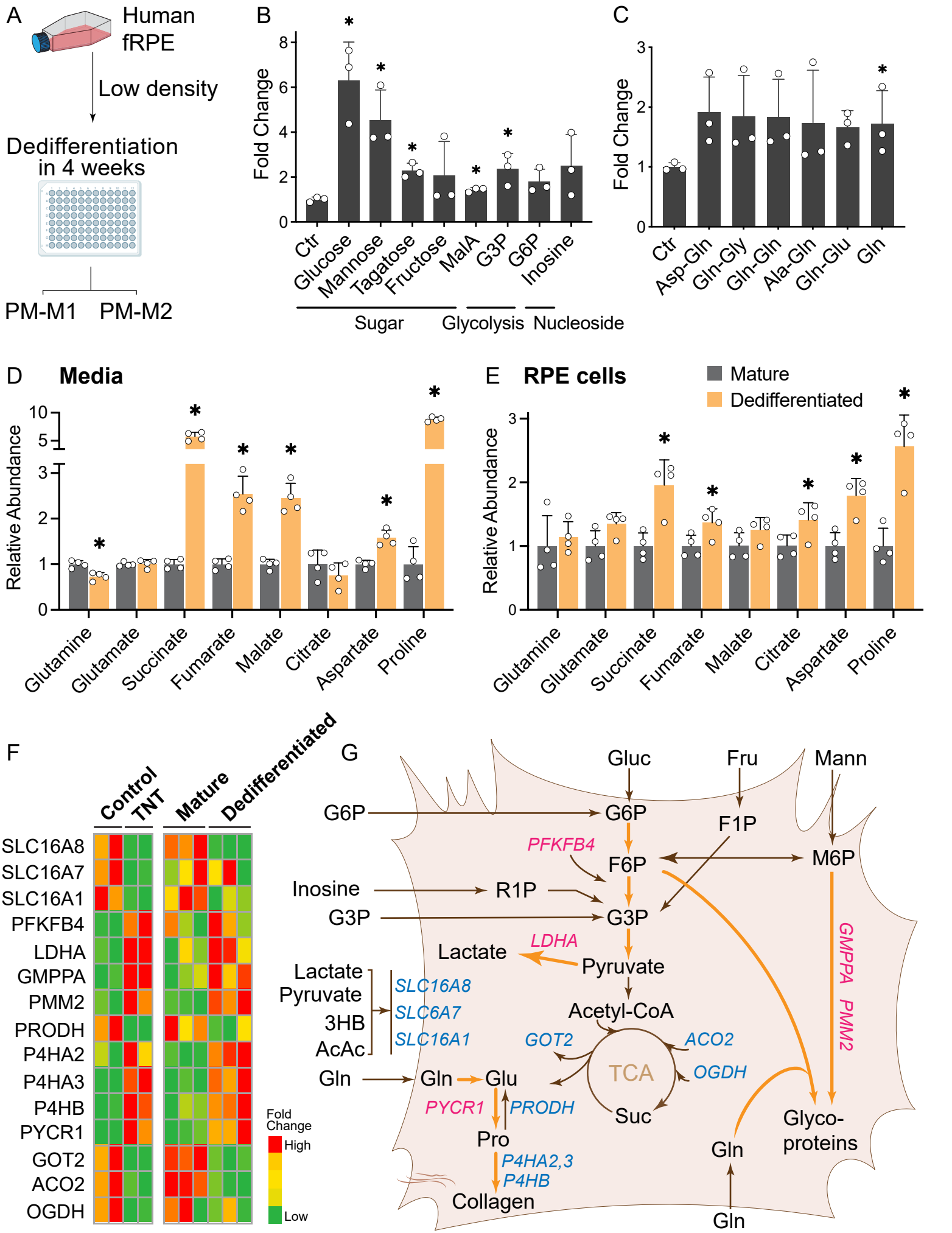
A
Human fRPE
Low density
Dedifferentiation in 4 weeks
PM-M1
PM-M2
B
Fold Change
Ctr
Glucose
Mannose
Tagatose
Fructose
MalA
G3P
G6P
Inosine
Sugar
Glycolysis
Nucleoside
C
Fold Change
Ctr
Asp-Gln
Gln-Gly
Gln-Gln
Ala-Gln
Gln-Glu
Gln
D
Media
Relative Abundance
Glutamine
Glutamate
Succinate
Fumarate
Malate
Citrate
Aspartate
Proline
E
RPE cells
Mature
Dedifferentiated
Relative Abundance
Glutamine
Glutamate
Succinate
Fumarate
Malate
Citrate
Aspartate
Proline
F
Control
TNT
Mature
Dedifferentiated
SLC16A8
SLC16A7
SLC16A1
PFKFB4
LDHA
GMPPA
PMM2
PRODH
P4HA2
P4HA3
P4HB
PYCR1
GOT2
ACO2
OGDH
Fold Change
High
Low
G
Gluc
Fru
Mann
G6P
G6P
F1P
PFKFB4
F6P
M6P
Inosine
R1P
G3P
G3P
LDHA
Lactate
Pyruvate
Lactate
Pyruvate
3HB
AcAc
SLC16A8
SLC6A7
SLC16A1
Acetyl-CoA
GOT2
ACO2
TCA
OGDH
Gln
Gln
Glu
PYCR1
PRODH
Suc
Pro
P4HA2,3
P4HB
Collagen
Gln
Glyco-proteins
GMPPA
PMM2
Gln

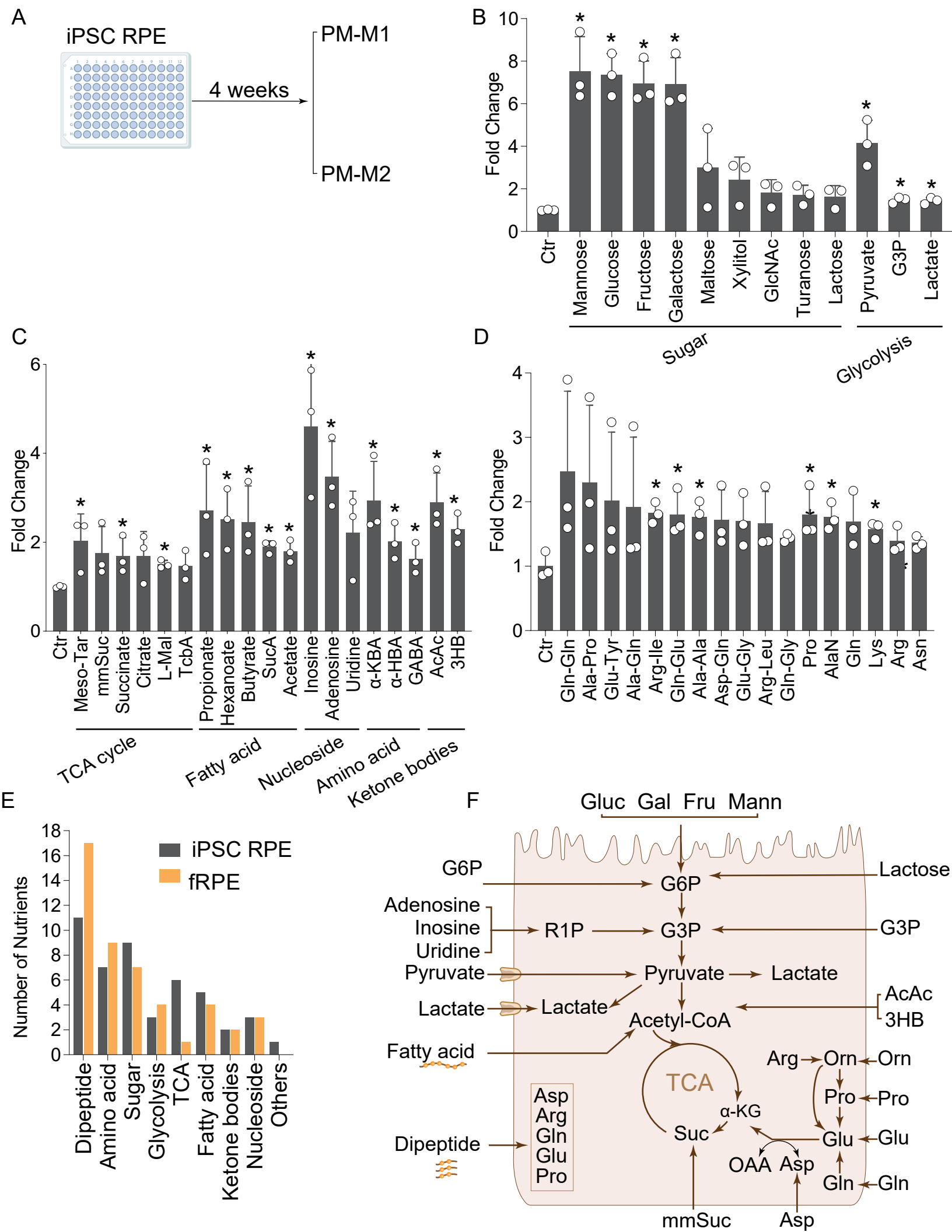
A
iPSC RPE
4 weeks
PM-M1
PM-M2
B
Fold Change
Ctr
Mannose
Glucose
Fructose
Galactose
Maltose
Xylitol
GlcNAc
Turanose
Lactose
Pyruvate
G3P
Lactate
Sugar
Glycolysis
C
Fold Change
Ctr
Meso-Tar
mmSuc
Succinate
Citrate
L-Mal
TcbA
Propionate
Hexanoate
Butyrate
SucA
Acetate
Inosine
Adenosine
Uridine
α-KBA
α-HBA
GABA
AcAc
3HB
TCA cycle
Fatty acid
Nucleoside
Amino acid
Ketone bodies
D
Fold Change
Ctr
Gln-Gln
Ala-Pro
Glu-Tyr
Ala-Gln
Arg-Ile
Gln-Glu
Ala-Ala
Asp-Gln
Glu-Gly
Arg-Leu
Gln-Gly
Pro
AlaN
Gln
Lys
Arg
Asn
E
Number of Nutrients
iPSC RPE
fRPE
Dipeptide
Amino acid
Sugar
Glycolysis
TCA
Fatty acid
Ketone bodies
Nucleoside
Others
F
Gluc Gal Fru Mann
G6P
Lactose
G6P
Adenosine
Inosine
Uridine
R1P
G3P
G3P
Pyruvate
Pyruvate
Lactate
Lactate
Lactate
AcAc
3HB
Acetyl-CoA
Fatty acid
Arg
Orn
Orn
TCA
Pro
Pro
α-KG
Asp
Arg
Gln
Glu
Pro
Suc
Glu
Glu
Dipeptide
OAA
Asp
Gln
Gln
mmSuc
Asp

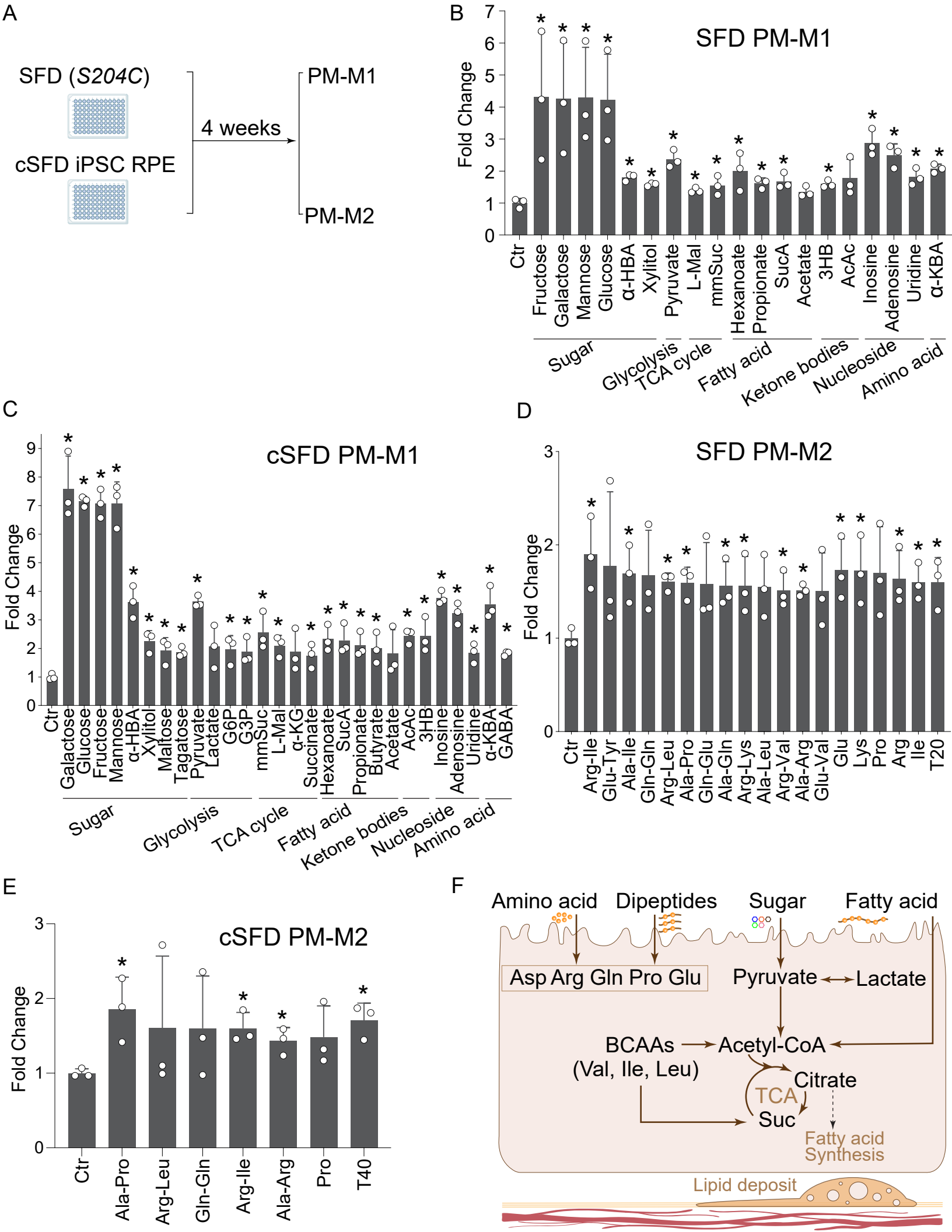
A
SFD (S204C)
cSFD iPSC RPE
4 weeks
PM-M1
PM-M2
B
SFD PM-M1
Fold Change
Ctr
Fructose
Galactose
Mannose
Glucose
α-HBA
Xylitol
Pyruvate
L-Mal
mmSuc
Hexanoate
Propionate
SucA
Acetate
3HB
AcAc
Inosine
Adenosine
Uridine
α-KBA
Sugar
Glycolysis
TCA cycle
Fatty acid
Ketone bodies
Nucleoside
Amino acid
C
cSFD PM-M1
Fold Change
Ctr
Galactose
Glucose
Fructose
Mannose
α-HBA
Xylitol
Maltose
Tagatose
Pyruvate
Lactate
G6P
G3P
mmSuc
L-Mal
α-KG
Succinate
Hexanoate
SucA
Propionate
Butyrate
Acetate
AcAc
3HB
Inosine
Adenosine
Uridine
α-KBA
GABA
Sugar
Glycolysis
TCA cycle
Fatty acid
Ketone bodies
Nucleoside
Amino acid
D
SFD PM-M2
Fold Change
Ctr
Arg-Ile
Glu-Tyr
Ala-Ile
Gln-Gln
Arg-Leu
Ala-Pro
Gln-Glu
Ala-Gln
Arg-Lys
Ala-Leu
Arg-Val
Ala-Arg
Glu-Val
Glu
Lys
Pro
Arg
Ile
T20
E
cSFD PM-M2
Fold Change
Ctr
Ala-Pro
Arg-Leu
Gln-Gln
Arg-Ile
Ala-Arg
Pro
T40
F
Amino acid
Dipeptides
Sugar
Fatty acid
Asp Arg Gln Pro Glu
Pyruvate
Lactate
BCAAs
(Val, Ile, Leu)
Acetyl-CoA
Citrate
TCA
Suc
Fatty acid
Synthesis
Lipid deposit

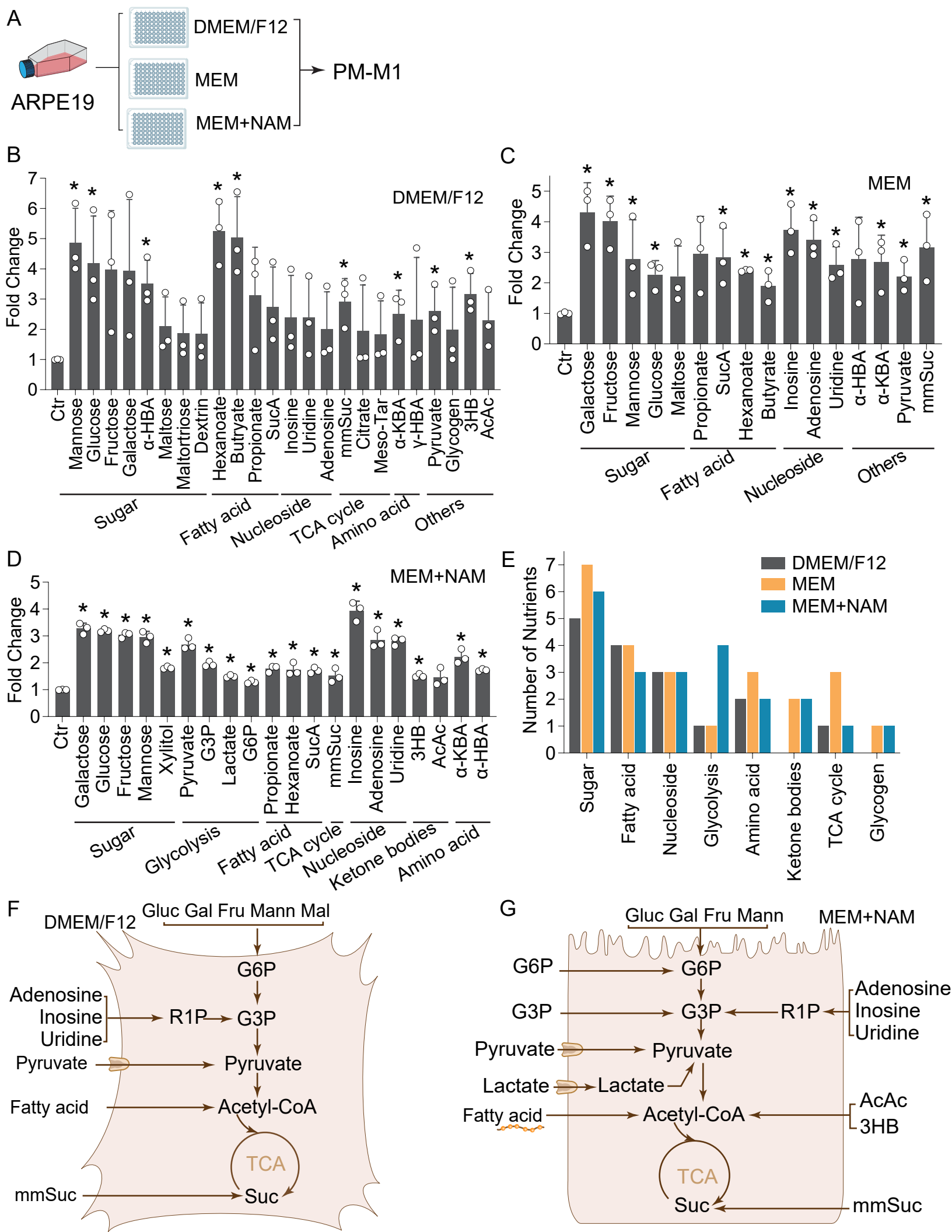
A
ARPE19
DMEM/F12
MEM
MEM+NAM
PM-M1
B
DMEM/F12
Fold Change
Ctr
Mannose
Glucose
Fructose
Galactose
α-HBA
Maltose
Maltortriose
Dextrin
Hexanoate
Butryate
Propionate
SucA
Inosine
Uridine
Adenosine
mmSuc
Citrate
Meso-Tar
α-KBA
γ-HBA
Pyruvate
Glycogen
3HB
AcAc
Sugar
Fatty acid
Nucleoside
TCA cycle
Amino acid
Others
C
MEM
Fold Change
Ctr
Galactose
Fructose
Mannose
Glucose
Maltose
Propionate
SucA
Hexanoate
Butyrate
Inosine
Adenosine
Uridine
α-HBA
α-KBA
Pyruvate
mmSuc
Sugar
Fatty acid
Nucleoside
Others
D
MEM+NAM
Fold Change
Ctr
Galactose
Glucose
Fructose
Mannose
Xylitol
Pyruvate
G3P
Lactate
G6P
Propionate
Hexanoate
SucA
mmSuc
Inosine
Adenosine
Uridine
3HB
AcAc
α-KBA
α-HBA
Sugar
Glycolysis
Fatty acid
TCA cycle
Nucleoside
Ketone bodies
Amino acid
E
Number of Nutrients
DMEM/F12
MEM
MEM+NAM
Sugar
Fatty acid
Nucleoside
Glycolysis
Amino acid
Ketone bodies
TCA cycle
Glycogen
F
DMEM/F12
Gluc Gal Fru Mann Mal
G6P
Adenosine
Inosine
Uridine
R1P
G3P
Pyruvate
Pyruvate
Fatty acid
Acetyl-CoA
TCA
mmSuc
Suc
G
MEM+NAM
Gluc Gal Fru Mann
G6P
G6P
G3P
G3P
R1P
Adenosine
Inosine
Uridine
Pyruvate
Pyruvate
Lactate
Lactate
Fatty acid
Acetyl-CoA
AcAc
3HB
TCA
Suc
mmSuc

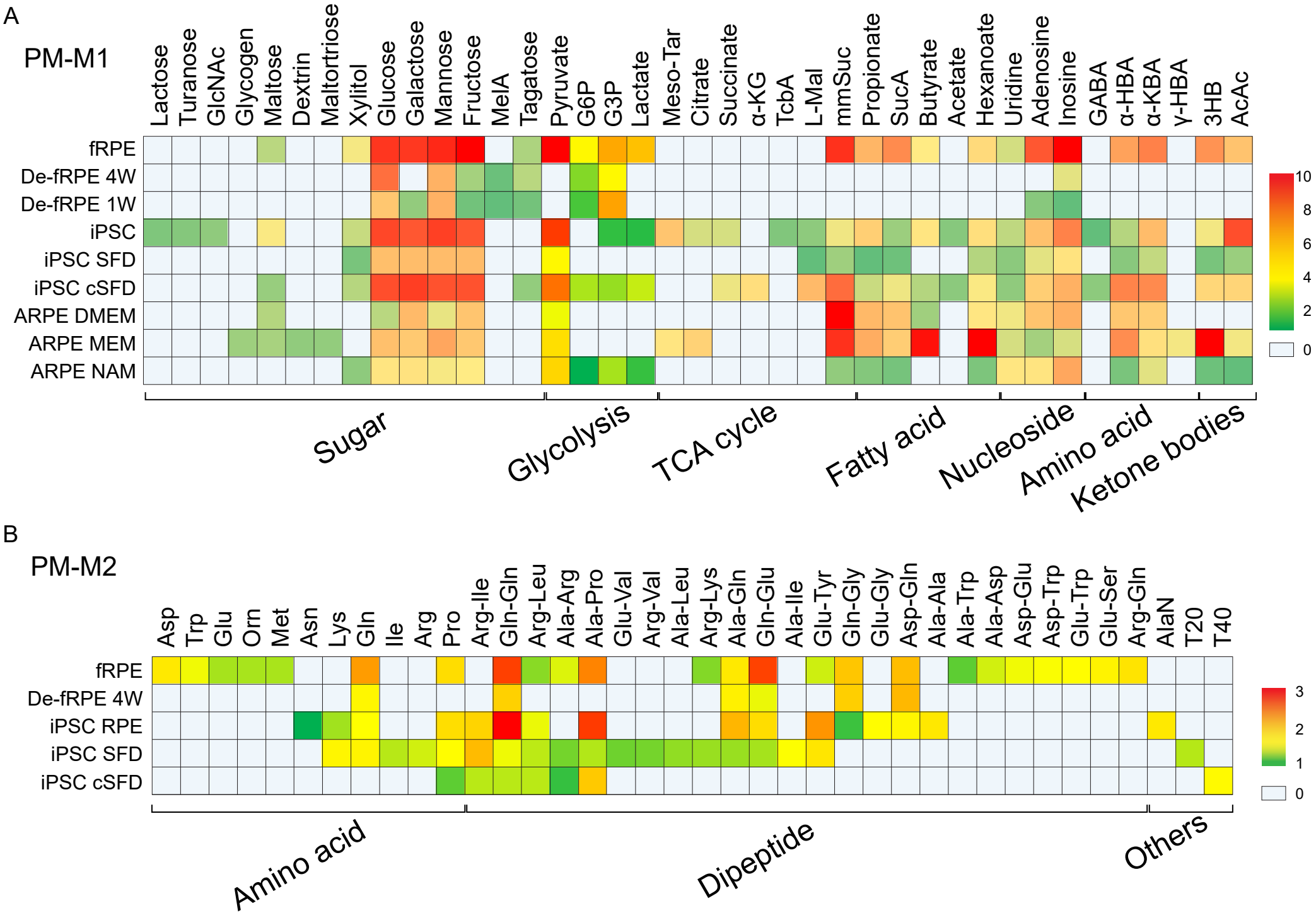
A
PM-M1
Lactose
Turanose
GlcNAc
Glycogen
Maltose
Dextrin
Maltortriose
Xylitol
Glucose
Galactose
Mannose
Fructose
MelA
Tagatose
Pyruvate
G6P
G3P
Lactate
Meso-Tar
Citrate
Succinate
α-KG
TcbA
L-Mal
mmSuc
Propionate
SucA
Butyrate
Acetate
Hexanoate
Uridine
Adenosine
Inosine
GABA
α-HBA
α-KBA
γ-HBA
3HB
AcAc
fRPE
De-fRPE 4W
De-fRPE 1W
iPSC
iPSC SFD
iPSC cSFD
ARPE DMEM
ARPE MEM
ARPE NAM
10
8
6
4
2
0
Sugar
Glycolysis
TCA cycle
Fatty acid
Nucleoside
Amino acid
Ketone bodies
B
PM-M2
Asp
Trp
Glu
Orn
Met
Asn
Lys
Gln
Ile
Arg
Pro
Arg-Ile
Gln-Gln
Arg-Leu
Ala-Arg
Ala-Pro
Glu-Val
Arg-Val
Ala-Leu
Arg-Lys
Ala-Gln
Gln-Glu
Ala-Ile
Glu-Tyr
Gln-Gly
Glu-Gly
Asp-Gln
Ala-Ala
Ala-Trp
Ala-Asp
Asp-Glu
Asp-Trp
Glu-Trp
Glu-Ser
Arg-Gln
AlaN
T20
T40
fRPE
De-fRPE 4W
iPSC RPE
iPSC SFD
iPSC cSFD
3
2
1
0
Amino acid
Dipeptide
Others